Carbohydrate Polymers 230 (2020) 115646

Contents lists available at ScienceDirect

Carbohydrate Polymers

journal homepage: www.elsevier.com/locate/carbpol

Anti-biofilm investigation of graphene/chitosan nanocomposites against biofilm producing *P. aeruginosa* and *K. pneumoniae*

Muthuchamy Maruthupandy[a], Govindan Rajivgandhi[b,d,e,*], Shine Kadaikunnan[c], Thangasamy Veeramani[d], Naiyf S. Alharbi[c], Thillaichidambaram Muneeswaran[a], Jamal M. Khaled[c], Wen Jun-Li[b,e], Khalid F. Alanzi[c]

[a] Laboratorio de Nanocelulosa y Biomateriales, Departamento de Ingeniería Química, Biotecnología y Materiales, Facultad de Ciencias Físicas y Matemáticas, Universidad de Chile, Avenida Beauchef 851, Santiago, Chile
[b] State Key Laboratory of Biocontrol and Guangdong Provincial Key Laboratory of Plant Resources, School of Life Sciences, Sun Yat-Sen University, Guangzhou, 510275, PR China
[c] Department of Botany and Microbiology, College of Science, King Saud University, Riyadh 11451, Saudi Arabia
[d] Medical Microbiology & Marine Pharmacology Laboratory, Department of Marine Science, Bharathidasan University, Tiruchirappalli 620 024, Tamil Nadu, India
[e] Southern Marine Science and Engineering Guangdong Laboratory (Zhuhai), Zhuhai 519000, PR China

ARTICLE INFO

Keywords:
Graphene/chitosan nanocomposites
Biofilm
Multi drug resistant bacteria
Urinary tract infection
Lethal effect

ABSTRACT

In this study graphene/chitosan nanoparticles (GR/CS NCs) were developed. The homogenous combination of GR and CS was confirmed by FTIR spectroscopy. The combination of CS with GR sheets reduced the XRD intensity of the GR peak in GR/CS NCs, while TEM images revealed the immobile CS coating of GR sheets. Further, the anti-biofilm activity of GR/CS NCs was tested. The tests showed that the formation of biofilm by *Pseudomonas aeruginosa* and *Klebsiella pneumoniae* was inhibited at 40□g/mL GR/CS NCs up to 94 and 92 %, respectively. The intracellular and cell surface damage of the bacteria was observed by CLSM and SEM. Also, GR/CS NCs produced a toxic effect of 90 % on *Artemia franciscana* at 70□g/mL upon 24 h incubation. The recorded properties of the synthesized GR/CS NCs qualify them as potential agents against multi-drug resistant bacteria.

1. Introduction

The urinary tract infections (UTIs) with associated biofilms are difficult due to the development of resistance to current antibiotics and immune system responses (Gupta, Singh, & Khan, 2017). Many bacteria are capable of forming biofilms on abiotic surfaces, which is one of the most important factors underlying the transformation of acute to chronic infections (Gurunathan, Han, Kwon, & Kim, 2014). According to the National Institute of Health and Center of Disease Control, approximately 65–80 % infectious diseases are caused by biofilm forming bacteria including the Gram-negative bacteria (GNB) of *Escherichia coli*, *P. aeruginosa*, *K. pneumoniae*, *Proteus mirabilis*, and Gram-positive bacteria (GPB) of *Staphylococcus aureus, Enterococcus, Bacillus* sp. (Shi et al., 2016; Yadav et al., 2017a, 2017b). Current commercially available antibiotics are ineffective in treating infections with biofilms and may allow for recurrent UTIs. These biofilms can be made by one or many bacterial species and show high antimicrobial tolerance compared to planktonic cultures (Santhosh & Kandasamy, 2015), thus biofilm-related infections are extremely difficult to treat and can cause urinary tract obstruction, urinary catheter or bladder blockage, bacteriuria, crystalline biofilms, urinary stones, pyelonephritis, and septicemia. In addition, it can contain unique virulence factors including efflux pump, quarum sensing molecules and enzymatic reaction products (Cady et al., 2012). The excretion of toxic materials and waste products from bacterial cells is regulated by the efflux system, which includes membrane-bound transporters with specific substrates and high drug exclusion capacity. The production of hydrolytic enzymes in GNB are the most lead causative agents for antibiotic resistance in biofilm forming bacteria, called β-lactamases (Prestinaci, Pezzotti, & Pantosti, 2015). All these factors and sustained unfavorable environments lead to the emergence of multi drug resistant bacteria (MDRB). Treating antibiotic-tolerant microbial biofilms requires the long-term use of high doses of antibiotics and results are not always satisfactory, largely due to limited antibiotic penetration or their ineffectiveness against resistant bacteria

* Corresponding author at: State Key Laboratory of Biocontrol and Guangdong Provincial Key Laboratory of Plant Resources, School of Life Sciences, Sun Yat-Sen University, Guangzhou, 510275, PR China.
E-mail address: rajivgandhimicro@yahoo.com (R. Govindan).

https://doi.org/10.1016/j.carbpol.2019.115646
Received 23 July 2019; Received in revised form 16 November 2019; Accepted 18 November 2019
Available online 22 November 2019
0144-8617/

(Hsu et al., 2008). To address this problem, we have designed novel and innovative chitosan (CS)-containing nanocomposites as alternative tools for destroying or damaging biofilms and eliminating MDRB. The general mechanisms of antimicrobial activity could be clear according to the target component of the bacterial cell against which it has its main activity (Krajewska, Kyzioł, & Wydro, 2013; Raafat & Sahl, 2009).

CS is the most important natural biopolymer and abundant source as it is consequent from the seashells of crustaceans on earth. It was explored widely for numerous years for practice in wound healing, tissue regeneration, bone alternates, waste water treatment and biosensor (Zhao et al., 2012). It is exciting properties contain numerous functional cluster, biocompatibility, biodegradability, and solubility in water medium (Fernandes et al., 2010; Ionita & Iovu, 2011; Venkatesan & Kim, 2010). Although, the various compensations and distinctive properties of CS, the deprived mechanical properties limit its usage in an extensive variety of fields. An active approach for refining the physical and mechanical properties of CS is to arrange biological-chemical materials mediated composites through the combination of grouts.

Graphene (GR) as an example of two-dimensional carbon arrangement was deliberated as a supreme nanostructure. GR has essential electrical and mechanical properties that build them supreme for nanostrengthening in CS polymer, which were multifaceted applications (Guo et al., 2011; Jeon, An, & Jeong, 2012; Potts, Dreyer, Bielawski, & Ruoff, 2011). Additionally, GR has been found to outstrip as supporting grout (Rafiee et al., 2009) and noble biocompatibility (Syama & Mohanan, 2016). Raafat and Sahl (2009) and Hu et al. (2010) novelty stated the antibacterial efficiency of CS, GR and GR-based materials considerably inhibited the bacterial growth and motivated by this distinct properties are the reason for selected this investigation. Conversely, the application of GR as a supporting substantial in the CS medium is still narrow since it is problematic to disperse GR in the CS medium. Graphene/chitosan nanocomposites (GR/CS NCs) have exposed an enhancement in mechanical properties over pure CS (Lau, Cooney, & Atanassov, 2008; Potts et al., 2011).

In this present study, we examined the effect of synthesized GR/CS NCs on biofilm formation using by the selected uropathogens *P. aeruginosa, K. pneumoniae.* In addition, the toxicity of the GR/CS NCs was evaluated against marine model organism *A. franciscana.* We also determined that such assays using GR/CS NCs yielded relatively accurate and consistent results. Consequently, GR/CS NCs could be an economical and rapid way to disrupt biofilms and treat bacterial infections.

2. Materials and methods

2.1. Materials and chemicals

Graphite powder (99.95 %) was purchased from Aladdin Industrial Corporation, China. Solution of 37 wt% hydrochloric acid (HCl), 98 wt % sulfuric acid (H_2SO_4), hydrogen peroxide (H_2O_2) and potassium permanganate ($KMnO_4$) were purchased from Sinopharm Chemicals and Reagent Co. Ltd, China. Chitosan powder with a molecular weight of 310,000–375,000 Da, a viscosity range of 800 − 2000 cP, and > 75 % deacetylation were purchased from Aladdin Industrial Corporation. and acetic acid from Richjoint Chemicals, China. 1-Ethyl-3-(3-dimethylaminopropyl) carbodiimide (EDC) and N-Hydroxysuccinimide (NHS) were obtained from Sigma Aldrich, China. All the chemicals were used as received without further purification. The deionized water was used throughout of this study. All reagents for biological assays involving chemicals and antibiotic discs were purchased from Sigma-Aldrich, India. The pathogens strains *P. aeruginosa* MTCC 2453 and *K. pneumoniae* MTCC 3384 were obtained from Microbial Type Culture Collection (MTCC), Mumbai, India.

2.2. Synthesis of graphene (GR)

The graphite oxide was synthesized using modified Hummer's method (Hummers & Offeman, 1958). Briefly, 1 g of graphite powder was added to 80 mL of H_2SO_4 and stirred in an ice bath for 30 min. Next, 6 g of $KMnO_4$ was slowly added to the reaction mixture and stirred again. The ice bath was then replaced by a 30–35 °C oil bath, and the solution was stirred overnight. The next day, 100 mL of water was slowly added and the mixture stirred for 30 min. A mixture of H_2O_2 (5 mL) and water (100 mL) was slowly added to the above solution and stirred for 10 min. The solution was gradually turned yellow from dark brown. The solution was then filtered to get the precipitate. The filtrated (graphite oxide) was initially washed (3–4 times) using HCl and then washed several times in H_2O until the neutral pH was reached. Synthesized graphite oxide was then dispersed in water and sonicated in bath sonicator at power of 150 W and frequency of 54 KHz for 4 h to get GO. In the typical synthesis, dried GO powder was dispersed in 90 mL of water (10 mg/mL) and sonicated for 30 min to obtain GR suspension.

2.3. Synthesis of GR/CS NCs

The GR/CS NCs were prepared using the modified protocol of Jia, Gai, Wang, and Zhao (2016). Concisely, 1 g of the CS and 200 mg of the GR were dispersed in 100 mL of water containing 1 % acetic acid solution using a bath sonication for 2 h. Next, 1.3 g of the 1-Ethyl-3-(3-dimethylaminopropyl) carbodiimide (EDC) and 1.6 g of the N-Hydroxysuccinimide (NHS) were added slowly to the reaction mixture and the combination of the solution was constantly stirred for 24 h. After the reaction completed, the suspension was filtered, the filtered precipitate was washed with 5 % acetic acid then deionized water in turn to remove excess CS, EDC and NHS from the reaction mixture. Additionally, the filter precipitate was dialyzed using deionized water for 3 days, and freeze-dried to obtain the GR/CS NC powder (Fig. 1).

2.4. Characterization of GR/CS NCs

The structure of the GR/CS NCs were examined using by a Fourier transform infrared spectrometer (FTIR, Spectrum 100, Perkin Elmer, U.S) at the wave number of 4000–400 cm^{-1}. Powder XRD of the synthesized samples was recorded by Rigaku D/max-RA X-ray diffract meter equipped with Cu-Ka radiation (λ = 1.54178 Å) at 2θ range between 10° and 80°. The structural morphology and chemical elemental analysis of the samples was observed using a scanning electron microscope with the voltage of 2.0 kV and magnifications range between 10,000× and 50,000×" (SEM, Hitachi S-4800). The surface morphology and size of the samples were investigated by transmission electron microscopy (TEM, Hitachi JEM-2100).

2.5. Detection of multi drug resistance profile

Fifty strains of Gram-negative bacteria known to cause UTIs were obtained from the Department of Microbiology, K.A.P.V. Government Medical College, Tiruchirappalli, Tamil Nadu, India. Based on the MDRs effect, *P. aeruginosa* and *K. pneumoniae* were selected for this study and grown in tryptic soy broth (TSB) at 37 °C for 24 h. After 24 h incubation, the ciprofloxacin resistant effect of the selected strains were detected by using the HEXA disc method (Rajivgandhi, Muneeswaran et al., 2018). For *P. aeruginosa,* the specific UTI panel discs of Pseudo 9 HX053 and Pseudo 12 HX103 were used, which included ceftazidime (CAZ-30 µg), ciprofloxacin (CIP-5 µg), Co-Trimoxazole (COT-25 µg), gentamycin (GEN-10 µg), imipenem (IPM-10 µg), ticarcillin/clavulanic acid (TCC-75/10 µg) and ciproflaxacin (CIP-5 µg), imipenem (IPM-10 µg), meropenem (MRP-10 µg), ertapenem (ETP-10 µg), cefoperazone/sulbactum (CFS-75/30 µg) piperacillin/tazobactam (PIT-100/10 µg). For *K. pneumoniae,* the the specific UTI panel discs of Kleb 1-

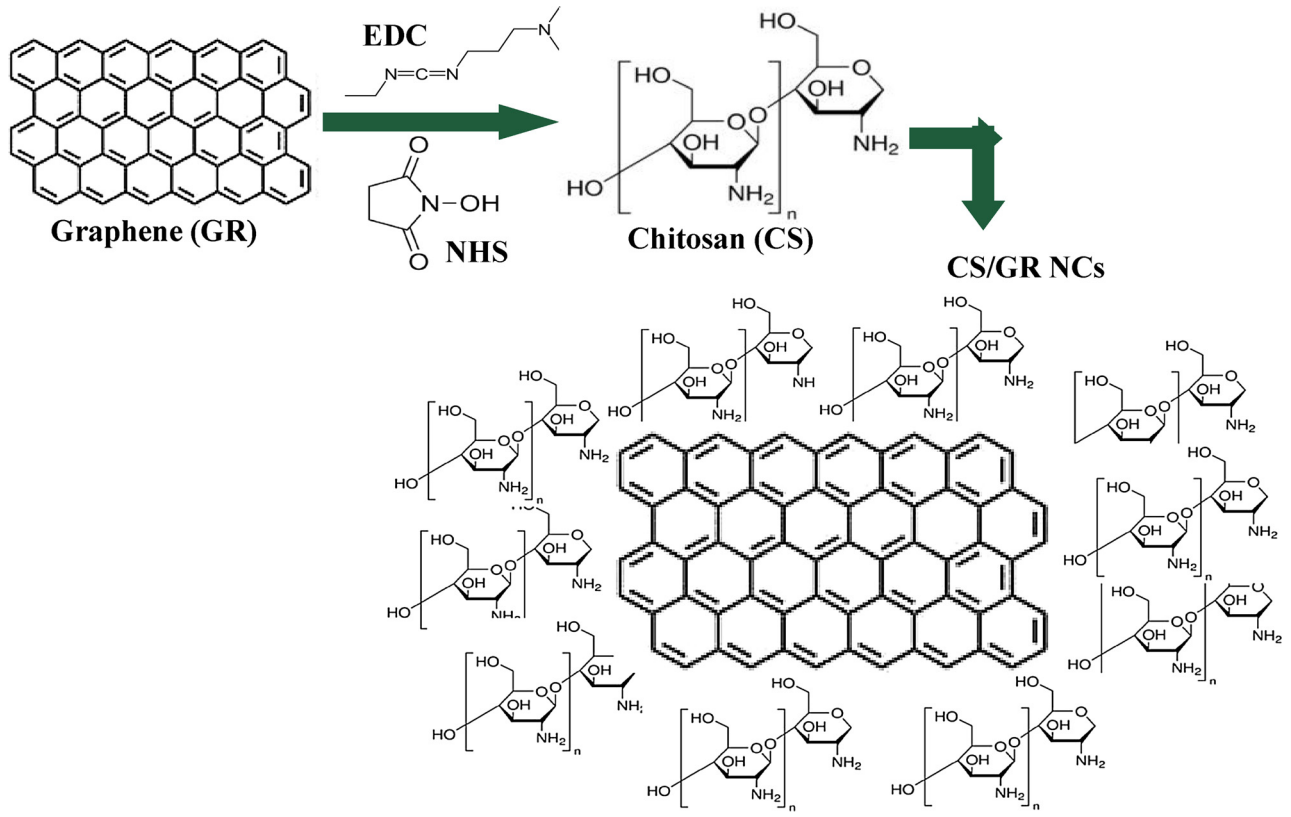

Fig. 1. Schematic reprasentation of EDC and NHS influced between graphene and chitosan crosslinking to produce GR/CS NCs.

HX033 and Kleb 2 - HX077 were used, which included nalidixic acid (NA-30 µg), nitrofurantoin (NT-300 µg), cephalothin (CEP-30 µg), ampicillin (AMP-25 µg), co-Trimoxazole (Cot-25 µg), norfloxacin (NX 10 µg) and amoxyclav (AMC-30 µg), ampicillin (AMP-10 µg), ciprofloxacin (CIP-5 µg), co-Trimoxazole (COT-25 µg), gentamicin (GEN-10 µg), norfloxacin (NX 10 µg).

2.6. Detection of biofilm formation

Based on the ciprofloxacin resistance ability, the selected uropathogens *P. aeruginosa, K. pneumoniae*, and non-biofilm forming *P.* aeruginosa MTCC 2453 and *K. pneumoniae* MTCC 3384 cultures were tested for detection of their biofilm forming ability by using the TCP assay and the CRA agar assays. Both the *P. aeruginosa* MTCC 2453 and *K. pneumoniae* MTCC 3384 cultures were served as reference strains for non-biofilm production.

2.6.1. Tissue culture plate method (TCP)

The biofilm formation of selected uropathogens were detected by TCP assay with96-well polystyrene plate (Rampelotto et al., 2018). Briefly, fresh TSB with 1 % glucose as inoculated with 100 µL of cultures produced from 24 h of growth in a 96-well plate and incubated at 37 °C for 24 h. Whereas, samples made without addition of bacteria were used as controls. After 24 h incubation, the plates were washed with 5 mL of phosphate buffered saline (PBS) to detach the free planktonic cells, then the remaining adherent bacterial cells on the plates were stained with 0.4 % crystal violet solution (w/v) for 15 min. The excess dye was rinsed off by washing thrice with deionized water and then allowed to dry. Finally, 1 mL of 90 % ethanol was added in to the wells and O.D value was calculated at 540 nm in Uv-spectrometer analysis (BioRad, Japan). Biofilm formation was confirmed based on OD_{570} values. This assay was performed in triplicate for each sample and the percentage of inhibition (PI) was calculated as follows with equation.

$$PI = (Control\ OD570nm\text{-}Test\ OD570\ nm) / Control\ OD570\ nm\ X\ 100 \quad (1)$$

2.6.2. Congo red agar assay (CRA)

The biofilm formation of control and test uropathogens were further confirmed by CRA method (Kaiser et al., 2013). Briefly, the treated and control cultures of both the uropathogens were directly inoculated on the CRA medium. These dilute cultures were then incubated at 37 °C for 24 h. After incubation, the black coloration around the colonies indicated biofilm production while pink colored colonies without such black coloration were said to lack biofilm production.

2.7. Antibacterial activity of GR and GR/CS NCs

The antibacterial activity of synthesized GR and GR/CS NCs against biofilm forming uropathogens of *P. aeruginosa, K. pneumoniae* were determined by the standard disc diffusion assay (de Moraes, Lima, de Faria, Brocchi, & Alves, 2015). Briefly, both the selected uropathogens were spread on Muller Hinton Agar (MHA) plates using sterile cotton swab. The 6 mm sterile discs were impregnated with various concentrations (5 – 100 µg/mL) of GR, GR/CS NCs and the discs were placed over the bacterial lawn. The sterile disc loaded with distilled water served as a control and the plates were incubated at 37 ℃ for 24 h. After 24 h, the zones of inhibition around the nanomaterial treated discs were observed and zones diameters measured (mm).

2.8. Anti-biofilm activity

An assay was performed to detect the ability of GR and GR/CS NCs to inhibit the biofilm formation in selected *P. aeruginosa, K. pneumoniae*. In this method, the incorporation of crystal violet into the fixed cells were analyzed by microtitre ELIZA reader analysis (Xu et al., 2017). Briefly, 100 µL of selected biofilm forming uropathogens of *P.*

aeruginosa, K. pneumoniae were added into the fresh tryptic soy broth (TSB) in 24 wells flat-bottom polystyrene plates. GR/CS NCs ranging in concentration from 5 − 50 μg/mL were added in the to the bacteria-containing wells and incubated at 37 ℃ for 24 h. After incubation, nonadherent cells were discarded and adherent cells thoroughly rinsed with sterile double distilled water to remove remaining non-adherent bacteria then air-dried. The biofilm was stained with 0.45 crystal violet solution (w/v) for 15 min. Then, the wells were washed three times with sterile distilled water to remove excess stain. The dye incorporated by the adherent cells were solubilized with 500 μL of 90 % ethanol was added into each well after drying. The absorbance of each well was measured at 540 nm using a microtiter ELISA reader. Bacterial samples lacking GR/CS NCs served as positive controls and media alone served as a blank. The absorbance differences between treated and control wells were considered as an index of bacterial adherence to the surface and thus the activity of biofilm. The methods were conducted in triplicate manner and the data are expressed as means ± SD. The percentage of inhibition (PI) was measured using equation.

PI = [Control OD 570 nm - Test OD 570 nm / Control OD 570 nm] X 100 (2)

2.9. Biofilm metabolic assay

To detection of metabolic respiratory activity, the 2,3-bis(2-methoxy-4-nitro-5 sulfophenyl)-2H-tetrazolium-5-carboxanilide (XTT) reduction method reduction assay (Hi-Media, India) was performed as previously described method of Huang, Liu, Yang, and Zhou (2019). After removing the non-adherent cells from both *P. aeruginosa* and *K. pneumoniae* samples in 24-well plates, the remaining biofilms were washed three times with PBS then covered in 10 μL of XTT solution (0.5 mg/mL) and incubated for 5 min at room temperature. Next, 1 μL of freshly prepared menadione acetone solution (1 mG/mL) and followed by 100 μL of PBS were added into the wells. All the plates were shaken well and incubated at 2 h at 37 °C in dark condition. The absorbance of the plates were measured at 540 nm using ELIZA reader (Shimadzu, Japan) and compared to control absorbance. All samples were assayed in triplicate and results were interpreted in terms of inhibition percentage using the following equation:

$$\% \text{ of inhibition} = 100\ (OD_{sample}\text{-}OD_{control}) \times 100 \quad (3)$$

The metabolic activity of decreased biofilm growth during the XTT assay was validated by using CRA plate method (Felipe et al., 2019). An aliquot of 0.1 mL of XTT wells were seeded onto the CRA plates without addition of the nanocomposites, and bacterial growth was calculated in order to determine metabolic activity levels in bacterial samples after 12 h of incubation. Results were considered indicative of antibacterial activity when colonies were either lower in number or not present on CRA plates of increasing XTT assay sample concentration. This approach was used to narrow down to the nanocomposite.

2.10. Microscopy based assays

2.10.1. Confocal laser scanning microscopy

The BIC of GR, and GR/CS NCs against biofilm forming uropathogens of *P. aeruginosa, K. pneumoniae* were observed by CLSM (Divya et al., 2018). The 100 mL overnight cultures of *P. aeruginosa, K. pneumoniae* were added into the 24 well plate containing sterilized TSB broth along with BIC of GR and GR/CS NCs. In addition, the sterile glass slides having the 1 × 1 cm dimension were kept in the same 24-well polystyrene plates. Whereas, without addition of culture containing broth with GR and GR/CS NCs glass slide acted as a control. All the plates were incubated at 37 °C for 24 h. After incubation, the culture was discarded and the cover slide was taken separately. After, the cover glasses were soaked into the PBS and wash with three times. Consequently, the cover glasses were washed with double distilled water for removal of excess stain. In the dark condition, 1 mg/mL acridine orange (AO) dye was added in the ration of 1:1. Finally, the stained cells of the treated and untreated cover glasses were analyzed by CLSM using 488 nm argon laser and 500–640 nm band pass emission filter.

2.10.2. Scanning electron microscopy

Morphological alteration of treated or untreated biofilm forming *P. aeruginosa* and *K. pneumoniae* at the BIC of GR, and GR/CS NCs was added in 10 mM PBS (pH7.4) at 37 °C for 24 h. After 24 h incubation, the cells were washed and then resuspended in10 mM sodium phosphate buffer (pH 7.4) and fixed with an equal volume of 4 % glutaraldehyde. The fixed cells were vacuum filtered onto 0.1 mm of polycarbonate membrane filters and subsequently, dehydrated in ethanol-graded series (10, 20, 30, 40, 50, 60, 70, 80, 90 and 100 %). The aluminum specimen support of mounted filter was coated with 15 nm thickness of gold-palladium metal (60:40 alloys). The samples were air dried and then analyzed by SEM (Cambridge Stereo scan 200 SEM) using an accelerating voltage of 20 kV (Shao et al., 2015).

2.11. Toxicity evaluation of GR and GR/CS NCs

Toxicity assays using *A. franciscana* were performed according to a previously published protocol (Sivasubramanian, Salini, Veera Ravi, & Karutha Pandian, 2019), with some modification. Briefly, the natural seawater was collected from open sea and filtered through 50 μm net for removed organic matters and maintained with 33 ppt salinity. This salt water was oxygenated by common air pump, which is used in ornamental fish culture at 27 – 28 °C, pH 7.5–8.5 in control room. Commercial brand of GSI (Great Salt Lake) *A. franciscana* cyst was hatched out in salt water and maintained stock culture in laboratory condition. The colloidal NCs samples were solubilized in a proportion of 0.5 mL–2 mL and saline solution to obtain stock solution with this concentration is zero (C0). Here, various concentrations (5, 10, 20, 30, 40. 50, 60 μg/mL) of GR and GR/CS NCs were used for this assay. 10 nauplii was designed as setup (A) and another 10 adults was designed as setup (B). The experiments were protected from light for 24 and 48 h. After the experimental period, the number of dead individuals were counted (eg. Inactive condition) by using a magnifying glass for very small nauplii. The toxicity of GR and GR/CS NCs were rated based on the nauplii or adult death, which was counted by observation of absence of swimming activity.

3. Results and discussion

3.1. Characterization of GR/CS NCs

FTIR analysis was used to estimate the chemical composition of prepared GR, CS and GR/CS NCs. The FTIR spectrum of the GR exhibited the distinctive chemical composition with extensive absorption's at around 3381 and 1630 cm^{-1} owed to the hydroxyl groups (−OH) of H_2O molecules and C=C bonds related with emaciated vibrations of unoxidized graphite domains. The peaks at 1721 and 1053 cm^{-1} were assigned to C=O and C−O−C groups respectively (Fig. 2a). The pure CS polymer was displayed bands at 3534 and 1671 cm^{-1} corresponding to −OH stretching band and showed a band at 2949 cm^{-1} corresponding to stretching of C=O groups. The bands at 1314 and 1432 cm^{-1} arise from stretching vibration corresponding to primary (CH_2OH) and secondary alcohol (CH−OH) compound. The band at 1590 cm^{-1} indicates the stretching vibration of NH group corresponding to nitriles. In the spectrum of GR/CS NCs, the peaks at 1625 cm^{-1} corresponds to a C=O stretching vibration. while the peak at 1053 cm^{-1} corresponds to stretching vibrations from the C=O of −NHCO− in glucosidic bonds. Compared to CS and GR spectra, the GR/CS spectra lacks the peak at 1596 cm^{-1} belonging to N−H bending of

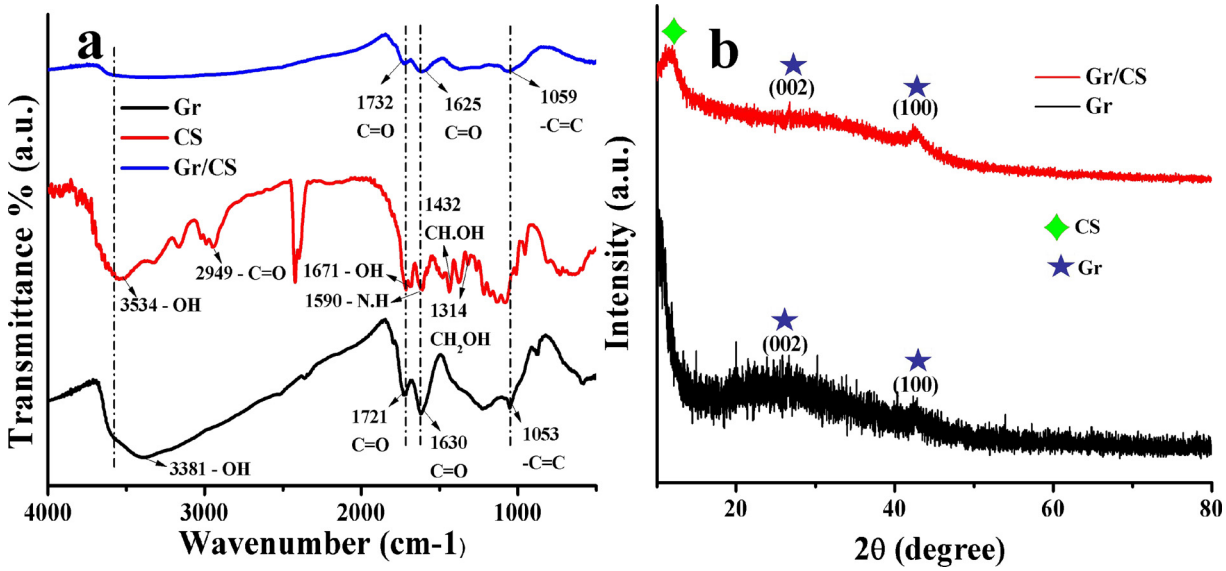

Fig. 2. FTIR spectra of GR, CS and GR/CS NCs (a), XRD pattern of GR and GR/CS NCs (b).

NH_2 groups and the band corresponding to the -NH_2 absorbance vibration group shifts to a higher wave number. The disappearance of the peak at 1721 cm^{-1} in the GR/CS spectra, corresponding to the C═O in carboxylic acid and carbonyl moieties in GR is likely too weak to be detect due to the mass ratio of GR to CS. These could be ascribed to the synergistic effect of hydrogen bonding between CS and the oxygenated groups in GR and electrostatic interaction between polycationic CS and the negative charge on the surface of GR (Li et al., 2013).

The XRD patterns of GR and GR/CS NCs are exposed in Fig. 2b. The XRD pattern of GR denoted two bands at 2θ value of 26° and 42°, which were assigned to the (002) and (100) planes, respectively. In the XRD pattern of GR/CS NCs, it was understandable that the contented of CS became greater and the depth of the peaks were associated with GR phase became superior as well (Wang, Shen, Zhang, & Tong, 2005). A vulnerable sharp peak of CS at the 2θ value 12° observed on the XRD pattern of GR−CS NCs made clear and confirmed that CS molecules were supported on the surface of GR surface (Fig. 2b black line). The decreased intensity of graphene (002) peak at 2θ value 26° in the GR−CS NCs (Fig. 2b red line) was due to the better density of the CS and consequently, the GR surface may be covered by means of CS. Hence, XRD results exhibited that the formation of CS on graphene surface. Additionally, no XRD pattern leaks were found except those corresponding to CS and GR, indicating successful synthesis and a lack of impurities. In this particular case, the electrostatic interaction and hydrogen bonding may contribute to a relatively ordered arrangement of the attached CS chains along the rigid template offered by GR (Jardón-Valadez, Bondar, & Tobias, 2014).

The physical appearance of GR and GR/CS NCs are shown in Fig. 3 a–d. The consistent discrete, sheet like morphology of GR was evidently visible in the SEM images. GR nanosheets were appeared to stick to each other and develop a film like morphology (Fig. 3 a, b). The morphological topographics of GR/Cs NCs were confirmed by SEM (Fig. 3 c,d). Fig. 3 c demonstrated that the rudimentary form of GR sheet was significantly exfoliated, and appeared like sheet or film like structure of one μm to several μm in length. Fig. 3 d shows an assessment of top of GR/CS NCs, which confirms that the CS polymer was closely reinforced at the external surface of GR sheets (Khan et al., 2016). For GR/CS NCs, the CS polymer backing on GR sheet surfaces reduced the van der Waals forces between GR sheets (Wang et al., 2018).

Structural differences between GR and GR/CS NCs were determined from TEM (Fig. 3 e–h). The consistently spread sheet like structure of GR nanosheet was clearly visible by TEM illustration (Fig. 3 e, f). Low and high magnification of TEM images (Fig. 3 g,h) confirmed that the CS was coated on GR sheets and the high magnification (Fig. 3 h), identically indicated that CS grow on GR sheets were in even and solid. The dimensions of CS on the GR sheets were showed variations in the extend of spreading. Based on the TEM results, after the unfluctuating GR/CS NCs was consequently exposed to a lengthy sonication, CS polymer motionless coated on the GR sheet with a high thickness after GR/CS NCs were sonicated for a lengthy period of time, suggesting a robust interaction network between the CS polymer and GR sheets.

3.2. Detection of multidrug resistance profile

The MDR effect of *P. aeruginosa and K. pneumoniae* were performed against was evaluated using the disc diffusion methods with various types of HEXA discs result (Fig. 4). During the Hexa disc antibiotic against *P. aeruginosa*, the co-trimoxazole and ertapenem of disc HX053 only produced inhibition zones of 6 mm and 4 mm of zone in HX053 and 10 mm and 6 mm zones in both HEXA discs of imipenem were observed respectively (Fig. 4a,b). In addition, ciprofloxacin of HEXA discs HX053 and HX103 produced 4 mm and 2 mm inhibition zones against *P. aeruginosa* was also observed. On the other hand, nitrofurantoin, cephalothin and ampicillin of the HX033 discs exhibited 4, 4, 6 mm of zone and ampicillin and amoxyclav of HX077 discs exhibited 4, 10 mm of zone against *K. pneumoniea* were observed respectively (Fig. 4c,d). While, ciprofloxacin of HEXA discs HX033 and HX077 produced 10, 8 mm zones against *K. pneumoniea* was also observed. The other tested discs were not produced any inhibition zones against both the uropathogens. From the observed results, it is clear that many antibiotic discs were ineffective against the selected uropathogens. Some tested Hexa discs exhibited minimum zones against both the uropathogens, but that zones were not reaching the sensitivity of the pathogens (Rajivgandhi et al., 2019). Based on the CLSI guidelines, both uropathogens were considered sensitive towards the antibiotics that created significant inhibitions zones, which likely arises from target site modifications of these antibiotics. In particular, the performance of β-lactams (ceftazidime), carbapenems (imipenem and meropenem) and fluoroquinolones (ciprofloxacin) classes of antibiotics were not able to performed better inhibition against these selected MDR uropathogens, in agreement with previous report of Olorunmola, Kolawole, and Lamikanra (2013). Among the three classes examined, ciprofloxacin from all tested HEXA discs consistently produced < 4 mm inhibition zones for both uropathogens. Our results therefore demonstrate that the selected uropathogens are MDR and possess ciprofloxacin resistance, likely due to the production of either ESBLs,

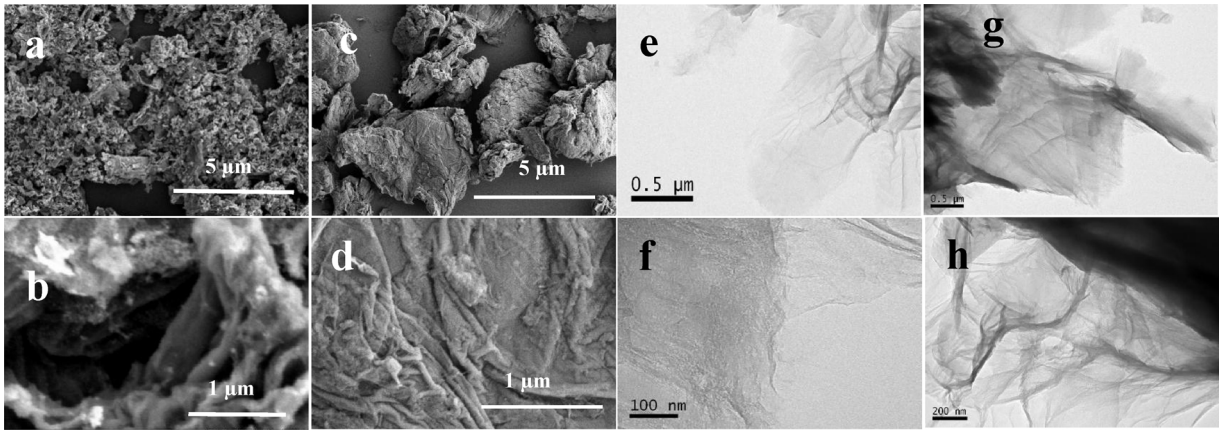

Fig. 3. SEM images of GR (a,b) and GR/CS NCs (c,d), TEM images of GR (e,f) and GR/CS NCs (g,h).

carbapenemases, or biofilms, which are associated with ciprofloxacin resistance. Ciprofloxacin-resistant bacteria have been shown to be extremely difficult to treat and pose a critical threat during infections due to a severe lack of viable treatment options (Zavrelova, Paterova, Gabalec, Zak, & Radocha, 2018) One potential mechanism underlying such resistance is the mutation of chromosomal genes to promote alterations in cell wall arrangements to prevent drug binding and decrease ciprofloxacin susceptibility. Ciprofloxacin is part of the fluoroquinolone class of broad-spectrum antibiotics and acts by inhibiting enzyme production in bacteria, thus altering the DNA replication, transcription, repair, strand supercoiling repair, and recombination (Redgrave, Sutton, Webber, & Piddock, 2014).

3.3. Detection of biofilm formation

Biofilm formation by the MDR strains *P. aeruginosa* and *K. pneumoniae* was examined using crystal violet staining, which yielded OD_{540} values of 0.454 for *P. aeruginosa* and 0.642 for *K. pneumoniae*, respectively after 24 h of incubation (Fig. 4i). In contrast, the control strains *P. aeruginosa* MTCC 2453 and *K. pneumoniae* MTCC 3384 exhibited the

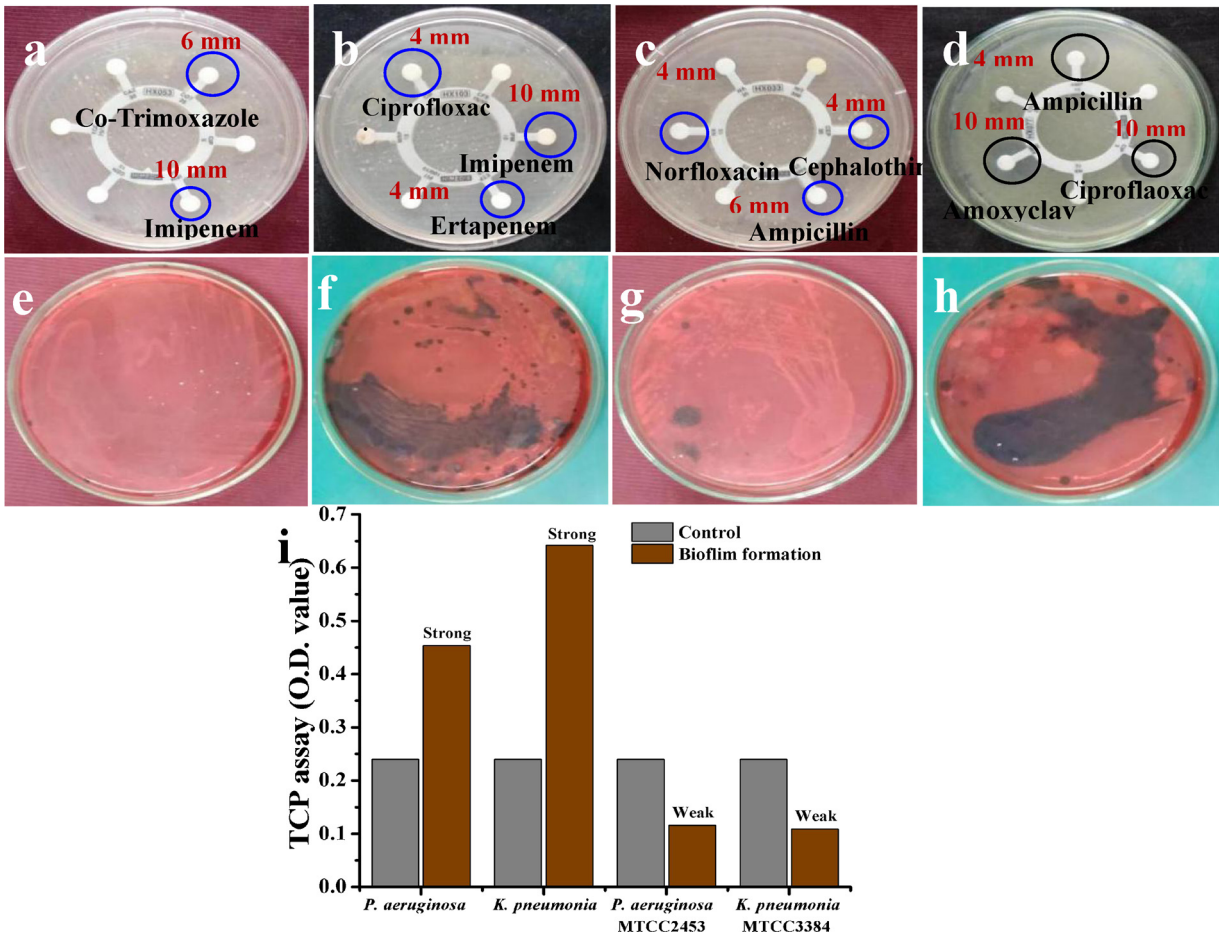

Fig. 4. Detection of antibiotic resistance *P. aeruginosa* against UTI panel discs of Pseudo 9 HX053 (a), Pseudo 12 HX103 (b) and *K. pneumoniae* against UTI panel discs of Kleb 9 HX033 (c), Kleb 1 UTI 9 HX077 (d). The biofilm formation of control strains of *P. aeruginosa* MTCC 2453 (e), *P. aeruginosa* (f), *K. pneumoniae* MTCC 3384 (g) and *K. pneumoniae* (h) in CRA medium. The O.D values of *P. aeruginosa* and *K. pneumoniae* strains in TCP assay for biofilm identification (i).

OD_{540} values of < 0.120. Based on these OD_{540} values, both selected uropathogens could produce biofilms with strong adherence efficiency when compared to control either produced no biofilms or biofilms with weak adherence (Abdel Halim, Kassem, & Mahmoud, 2018). In the TCP assay, only adherent cells were stained by crystal violet due to its selective binding of bacterial cells. The crystal violet staining method is a viable method to use estimation of adherent bacteria numbers. The primary finding of TCP assay proved, two tested strains were able to produce strong biofilm. This result was also further proved by CRA method (Rajivgandhi et al., 2014). Black color colonies present in the tested strains of CRA plates were confirmed, both uropathogens have the ability to form biofilm (Fig. 4f, h). Whereas, the pink color colonies of both the control strains indicated that the pathogens were inability to produce biofilm (Fig. 4e, g). The CRA method is used for detection of exopolysaccharide in the biofilm (Heidari et al., 2018), which is important for the survival of bacteria in biofilms. Exopolysaccharide functions include providing cell protection, enabling cell attachment to solid surfaces, enabling cell aggregation, and mediating cell-cell interactions. Results of both the TCP and CRA methods thus demonstrate that the MDR uropathogenic *P. aeruginosa* and *K. pneumoniae* strains chosen in this study are strong biofilm producers.

3.4. Antibacterial activity investigation of GR and G/CS NCs

The effect of GR and GR/CS NCs on MDR *P. aeruginosa* and *K. pneumoniae* were performed by agar well diffusion method and the result was presented in the Fig. 5. After 24 h incubation, the result revealed that the GR and GR/CS NCs were showed significant antibacterial efficiency against both the uropathogens. When compare to GR, GR/CS NCs showed better antibacterial activity against both the strains were observed. After 6 h of growth, 50 µg/mL of GR produced inhibition zones of 4 ± 1.0 mm and 6 ± 1.0 mm, while 30 µg/mL GR/CS NCs produced inhibition zones of 6 ± 1.0 and 8 ± 1.0 mm against *P. aeruginosa* and *K. pneumoniae* were observed respectively (Fig. 5a). After 12 h of growth, 50 µg/mL GR produced inhibition zones of 8 ± 1.0 mm and 12 ± 1.0 mm, while 30 µg/mL GR/CS NCs produced inhibition zones of 10 ± 1.0 mm and 15 ± 1.0 mm against *P. aeruginosa* and *K. pneumoniae* were observed respectively (Fig. 5a). Finally, after 24 h of growth, 50 µg/mL GR produced inhibition zones of 15 ± 1.0 mm and 21 ± 1.0 mm, while 30 µg/mL GR/CS NCs produced inhibition zones of 16 ± 1.0 mm and 19 ± 1.0 mm against *P. aeruginosa* and *K. pneumoniae* were observed respectively (Fig. 5a). In addition, increased concentrations of GR and GR/CS NCs produced increased growth inhibition of both uropathogens in a time-dependent manner, thus overall these results demonstrate that clearance zone size was dose- and time-dependent. Additionally, the MDR identification disc ciprofloxacin created no zone of inhibition for either pathogens, confirming that GR and GR/CS NCs are potentially excellent inhibitors of MDR pathogens. The result was agreed by Jiang et al. (2015), at different time interval, the chitosan mediated Gr NPs exhibited 55.92 % of inhibition against *E. coli* at 50 µg/mL,100 µg/mL and 200 µg/mL concentration was observed. In addition, the loss of cell viability was escalated with increasing exposure time interval. Recently, Di Giulio et al. (2018) and Yadav et al. (2017a,2017b) were also reported that the Gr NPs inhibited the pathogens of *S. aureus, E. coli* and *S. aureus, C. albicans* at increasing concentration. The recelt was most accordance with Pounraj, Prathap, and Paul (2018), Konwar, Kalita, Kotoky, & Chowdhury (2016), the GR/CS NCs showed excellent anti-bacterial activity against *E. coli, B. subtilis* and methicillin-resistant *S. aureus, E. coli* and *C. albicans* at 100 µg/mL. Therefore, the present result of our study was proved that the GR NPs and GR/Cs NCs were not only concentrated dependent but also time dependent.

3.5. Antibiofilm activity of GR and GR/CS NCs

In this study, we also examined the dose-dependent anti-biofilm effects of GR and GR/CS NCs towards *P. aeruginosa* and *K. pneumoniae* under *in vitro* conditions. After 24 h of incubation, bacterial cultures treated with either GR and GR/CS NCs showed inhibited biofilm formation compared to controls (Fig. 5b). Crystal violet complex was used to measured the biofilm reduction directly on the bottom of the microtitre plate. For all concentrations of GR and GR/CS NCs, biofilm formation was reduced compared to the control in a concentration-dependent manner and does not appear restricted to a particular bacterial species or set of growth conditions. *P. aeruginosa* and *K. pneumoniae* differ in their abilities to produce biofilms, as observed in this study. However, 92 % and 90 % reductions in biofilm production by *P. aeruginosa* and *K. pneumoniae* respectively, were observed upon treatment with 70 µg/mL of GR. Similarly, treatment with 40 µg/mL of GR/CS NCs created 94 % and 92 % reductions in biofilm formation by *P. aeruginosa* and *K. pneumoniae* respectively. Interestingly, comparable levels inhibition of biofilm activity were observed at significantly lower concentrations of GR/CS NCs compared to GR. Optimal biofilm disruption was observed at 70 µg/mL GR and 40 µg/mL GR/CS NCs (Fig. 5d), therefore these concentrations were labelled biofilm inhibition concentrations (BICs). Recently, it was reported that the dry black crystalline appearance of colonies of untreated *P. mirabilis* and *E. coli* cells indicated the production of exopolysaccharides, which are

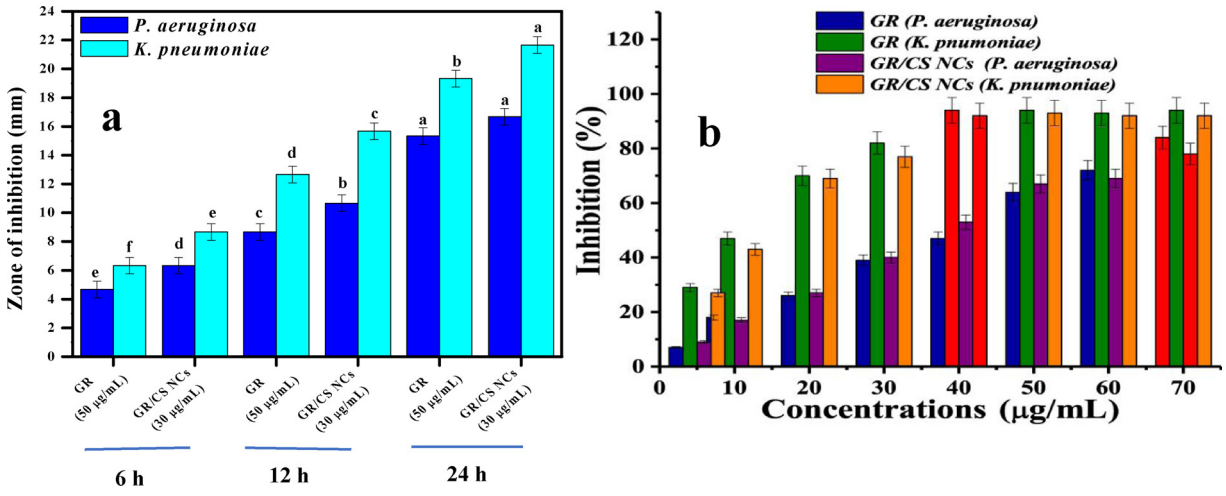

Fig. 5. Antimicrobial activity of GR and GR/CS NCs by various time interval (a) and the biofilm inhibition concentration of GR and GR/CS NCs against *P. aeruginosa* and *K. pneumoniae* (b). All the results were reported as mean ± standard deviation of three independent biological replicates. We employed ANOVA followed by Tukey's HSD test ($P \leq 0.05$) to analysis the data from our antibacterial activity with the help of the SPSS software package 16.0 version.

Table 1
Previous report of GR and Gr/CS NCs against biofilm forming bacteria at various concentration.

Samples	Test organisms	Various Concentrations	References
Gr NPs	*aureus and E. coli*	200 µg/mL	Yadav et al. (2017a,2017b)
Gr NPs	*S. aureus* and *C. albicans*	50 mg/mL	Di Giulio et al. (2018)
Gr NPs	*S. mutans*, *P. gingivalis* and *F. nucleatum*	100 mg/mL	He et al. (2015)
Gr/Cs NCs	*E. coli* and *B. subtilis*	100 mg/mL	Pounraj et al. (2018)
Gr/Cs NCs	*A. niger* and *B. subtilis*	200 µg/mL	Xu et al. (2017)
Gr/Cs NCs	Methicillin-resistant *S. aureus,* *E. coli* and *C. albicans*	100 µg/mL	Konwar et al. (2016)
GR NPs	*P. aeruginosa* and *K. pneumoniae*	75 µg/mL	Present study
GR/CS NCs	*P. aeruginosa* and *K. pneumoniae*	40 µg/mL	Present study

prerequisites for biofilm formation (Rajivgandhi, Maruthupandy, Muneeswaran, Anand, & Manoharan, 2018). In addition, the ZnO NS-treated strains could not produce dry crystalline black colonies due to an absence of exopolysaccharides, thus preventing biofilm formation. Yadav et al. (2017a,2017b) reported that the 200 µg/mL GR disrupted 90 % of biofilm formation by Gram-positive and Gram-negative due to reactive oxygen species (ROS)-mediated oxidative stress and inactivation of bacterial cell proliferation, which is required for biofilm formation. In addition, Di Giulio et al. (2018) demonstrated that the GR can penetrate into the polymeric matrix of biofilms and to destroy their three-dimensional structure, which induces cell detachment and interferes with microbial adhesion. Altogether, results from this study suggest that uropathogenic bacteria produce biofilms that are sensitive to GR and GR/CS NCs, causing cell death. So far, the mechanisms underlying GR and GR/CS NCs disruption of biofilm forming pathogens have been poorly understood, with evidence from previous reports listed in Table 1.

3.6. Biofilm metabolic assay

After 24 h incubation, 22 and 24 % and 6 and 8 % viable growths of Gr and GR/CS NCs treated *P. aeruginosa* and *K. pneumoniae* were observed respectively by XTT assay plates. Thus the evaluated strains showed higher sensitivity to GR/CS NCs compared to GR nanoparticles. The mechanistic approach of the nanomaterials led to a decrease in formazan production, it was suggested the reduction of metabolic activity. At the concentration of 70 µg/mL and 40 µg/mL of GR and GR/CS NCs were exhibited with 78 %, 76 % and 94 %, 92 % of inhibition against both the *P. aeruginosa* and *K. pneumoniae*, respectively. Nanomaterial concentrations resulting inhibition percentages are presented in in Fig. 6 a, b. The XTT results suggested that the synthesized nanomaterials were dose dependent against *P. aeruginosa* and *K. pneumoniae*. The XTT assay results were more correlated with viable count results in CRA medium. Further, the growth of nanomaterial treated plates was observed with drastically distributed colonies, whereas control plates growth were showed merged cells. For the confirmation of metabolic activity disruption, the CRA plates were showed with decreased black color colonies and increased pink color colonies at same BIC. The decreased black color of the treated cells of XTT wells were presented in Fig. 6 c. The result was exposed that the polysaccharide slime secreted in the biofilm matrix provides color variation due to the exopolysaccharide arrest. Contrary, the control strains of biofilm producing *P. aeruginosa* and *K. pneumoniae* plates were showed with black color colonies. Hence, the indirect and direct method of nanomaterials results were exhibited the effective inhibition on metabolic activity of selected biofilm producing *P. aeruginosa* and *K. pneumoniae.*

3.7. Morphological determination

3.7.1. Confocal laser scanning microscopy

Biofilm producing bacteria are surrounded by various membrane like exopolysaccharides for protects the cells from external agents (Nowacka, Rygała, Kręgiel, & Kowalewska, 2018). Thus, the membrane permeable drugs are very essential to inhibit the aggregation of cells each other (Subramaniyan, Ramani, Ganapathy, & Anbazhagan, 2018). The CLSM images of GR and GR/CS NCs against surface integrity of biofilm producing *P. aeruginosa* and *K. pneumoniae* were depicted in Fig. 7. At the BIC level of GR and GR/CS NCs, the crashed membrane molecules with dispersed cell arrangement were observed in treated uropathogens (Fig. 7c–f), whereas smooth, depicted well, intense adherent ability of untreated control cell were clearly showed in the AO stain and it images by CLSM (Fig. 7 a,b). The 3D structure (inset images) of GR and GR/CS NCs treated or untreated images were clearly indicated that the nanomaterials have antibiofilm activity against selected uropathogens. Here, AO is a fluorescent dye, which used for detection of attached or detached cells in the treated or control bacteria (El-kholany, Abielhassan, Elembaby, & Maria, 2012). The complete disruption 100 % of damaged cells were observed in BIC of GR/CS NCs than GR after 24 h incubation. The collapsed structures of dispersed cells was observed upon BIC treatment of GR and GR/CS NCs. It was clearly indicating that the presences of GR and GR/CS NCs have the biofilm inhibition effect against both uropathogens, which is higher for GR/CS. Finally, the NCs was localized within the cell membrane and rate of localization was higher in *P. aeruginosa,* compared with *K. pneumoniae.*

The CLSM images of the result clearly proved that the GR and GR/CS NCs were strongly degraded the aggregation of *P. aeruginosa, K. pneumoniae* via membrane damage which was stronger for GR/CS NCs compare to GR. The CLSM evidences were also indicated the potential effect of GR/CS NCs against *P. aeruginosa, K. pneumoniae.* However, the GR/CS NCs was a important material to inhibit the biofilm formation in high rate when compared with GR. Our result was most accordance with earliest report of Rajivgandhi, Maruthupandy et al. (2018), who reported that the biologically synthesized ZnO NSs was highly active at the concentration of 100 µg/mL against biofilm forming Gram negative bacteria. Our results are also previous work showing inhibition by ZnO NPs of biofilm formation at the irreversible adhesion stage and alterations of the bacterial membrane (Maruthupandy, Rajivgandhi, Muneeswaran, Song, & Manoharan, 2018).

3.7.2. Scanning electron microscopy

Membrane damage of GR and GR/CS NCs treated bacterial cells were further analyzed by SEM and the result is presented in Fig. 8. After 4 h of dehydration, the irregular surface, condensed cell membranes with compromised cellular death were observed in GR and GR/CS NCs treated bacteria (Fig. 8c–f). Whereas, smooth, rod shaped with intact cell wall of untreated control cells were also observed (Fig. 8a,b). At the

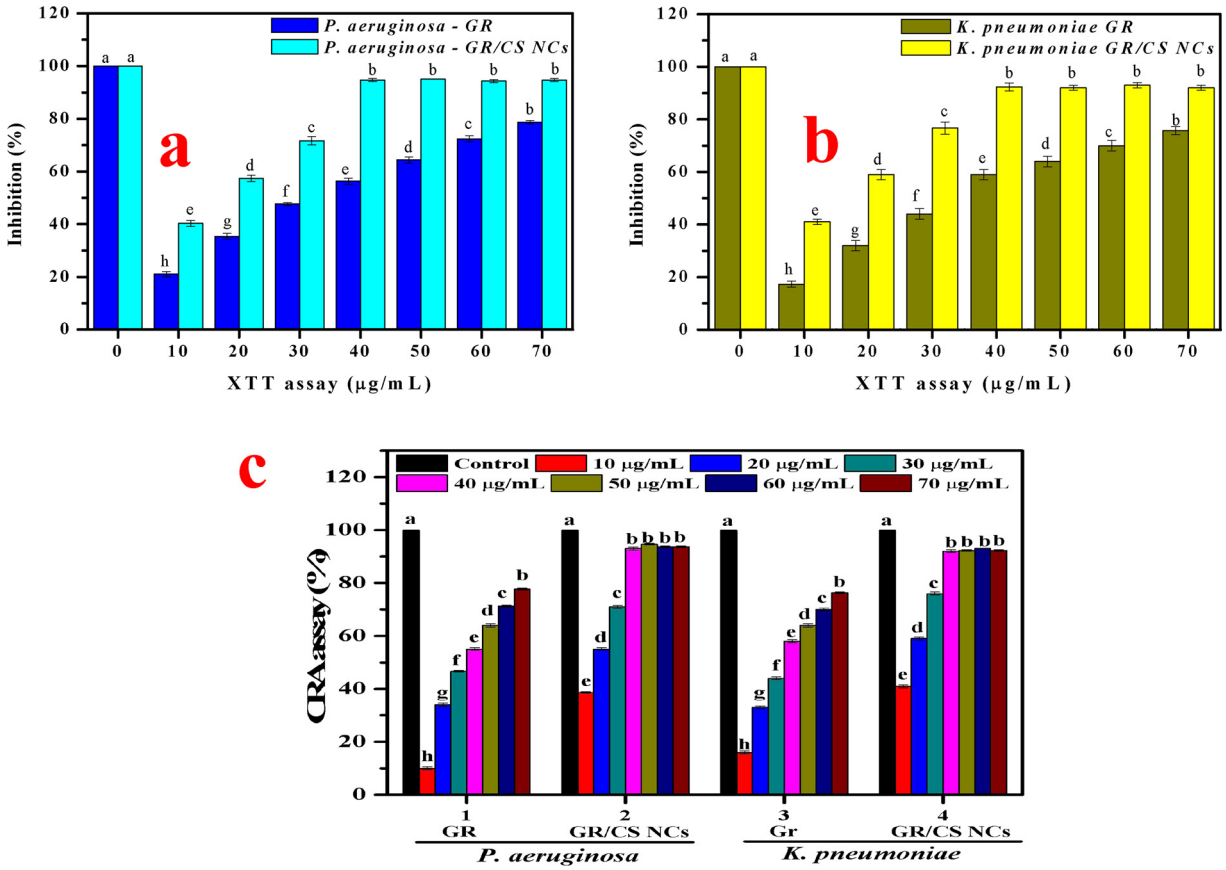

Fig. 6. The metabolic activity of GR and GR/CS NCs against *P. aeruginosa* (a) and *K. pneumoniae* (b) in XTT assay. The different color variation of Fig. 6 a, b were clearly indicated the inhibition effect of the GR and GR/CS NCs effect against both the *P. aeruginosa* and *K. pneumoniae*. The aliquot of XTT cultures of *P. aeruginosa* and *K. pneumoniae* (c) in CRA medium was observed for validation of bacterial viability of XTT assay. In the validation of Fig. 6c was indicated the exopolysachharide production ability of XTT resulted pathogens on CRA medium due to the black color production. All the results were reported as mean ± standard deviation of three independent biological replicates. We employed ANOVA followed by Tukey's HSD test ($P \leq 0.05$) to analysis the data from our metabolic activity with the help of the SPSS software package 16.0 version.

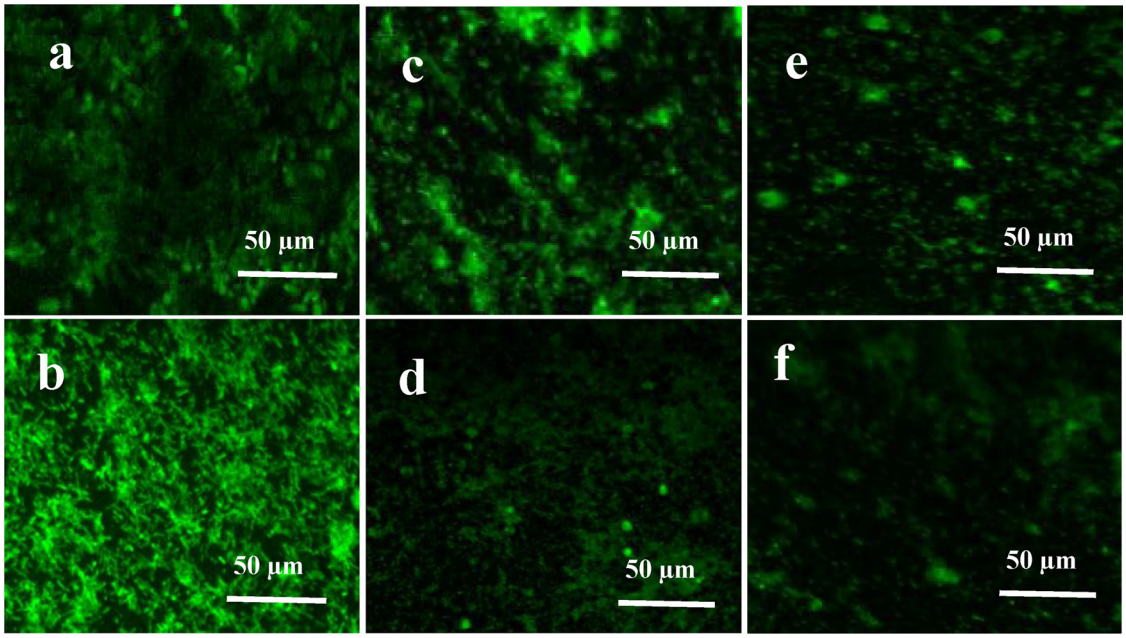

Fig. 7. Antibiofilm effect of untreated *P. aeruginosa* (a), *K. pneumoniae* (b) and GR and GR/CS NCs treated against *P. aeruginosa* (c, e), *K. pneumoniae* (d, f) were depicted respectively by CLSM.

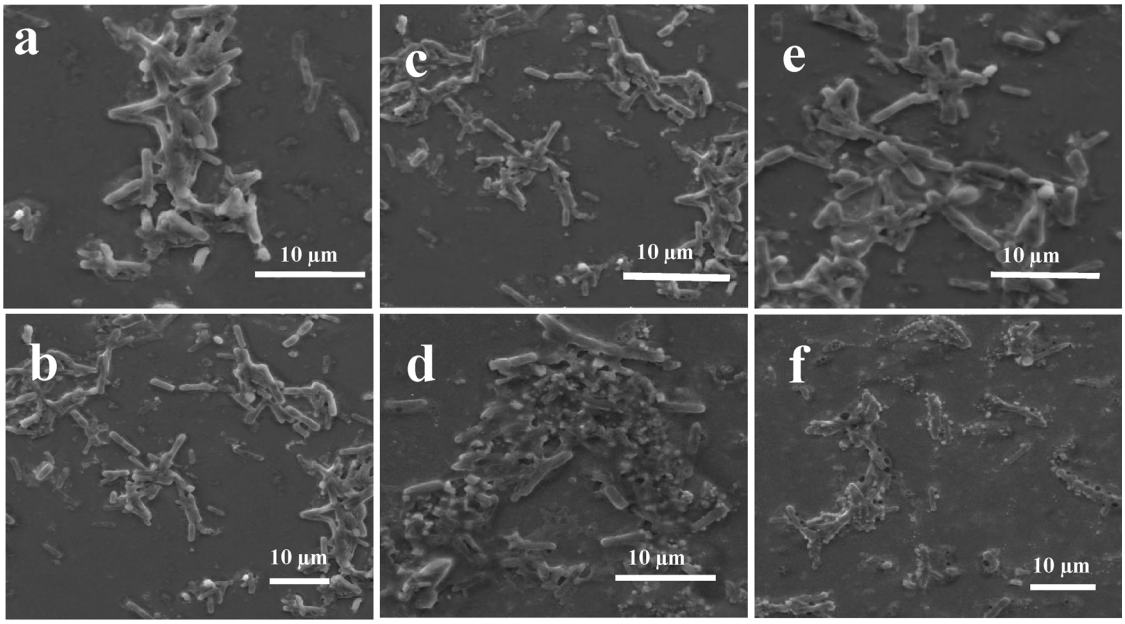

Fig. 8. Antibiofilm effect of untreated P. aeruginosa (a), K. pneumoniae (b) and GR and GR/CS NCs treated against P. aeruginosa (c, e), K. pneumoniae (d, f) were depicted respectively by SEM.

BIC of GR and GR/CS NCs were exhibited the irregular surface, membrane collapse, bleb formation and cell surface leakage for *P. aeruginosa* and wrinkled outer membranes damaged structure with losses of membrane integrity, inconsistent cellular content and leakages for *K. pneumoniae* were observed. Whereas, control cells showed no such evidence of structural defects. The attachment of the nanomaterials to the surface of gram negative bacterial cells has been previously examined and was shown to strongly disrupt the integrity of the bacterial membrane, thus making cells prone to cellular leakage and subsequent cell death (Budeli, Moropeng, Mpenyana-Monyatsi, & Momba, 2018). The dispersed nanomaterials were influenced in bacterial growth by targeting cell walls damage or folic acid and altering metabolic pathways, including protein or DNA replication (Hou et al., 2017). Our results thus demonstrate that GR and GR/CS NCs have strong antibiofilm activity towards select *P. aeruginosa* and *K. pneumoniae* strains and could be used as alternative antibiotic treatments in the medical field.

3.8. Toxicity evaluation of GR and GR/CS

The toxicity assay result was revealed, 50 % lethal doses (LD_{50}) or minimum lethal concentrations of GR and GR/CS NCs were observed against nauplii or adult after 24 h incubation. Compared to control of 10 nauplii or adult (Fig. 9a, b), the 6 number of mortality in GR treated samples were observed in Fig. 9c,d. The complete mortality (10) numbers were observed in GR/CS NCs samples at different concentration (Fig. 9e,f). Among the two nanomaterials, GR was exhibited 60 % of death against nauplii was observed at the concentration of 70 µg/mL (Fig. 9g). Whereas 68 % of *Artemia nauplii* martality rate at 40 µg/mL and 100 µg/mL at 70 µg/mL of GR/CS NCs were observed after 24 h of incubation, respectively (Fig. 9h).

Furthermore, the 40 % of GR treated adult *A. franciscana* lethal effect was observed at the concentration of 70 µg/mL (Fig. 9i), whereas 90 % of the GR/CS NCs treated *Artemia* adults died at aconcentration of 50 µg/mL (Fig. 9j) at 24 h respectively. The LC_{50} evaluation of GR and GR/CS NCs against the *Artemia* nauplii. The high toxicity effect in *Artimia* nauplii and low toxicity effect in *Artimia* adult were observed using GR and Gr/Cs NCs. These results indicated that the nanomaterials inhibits the *Artemia* in a concentration dependent manner and and show that GR/CS NCs were more toxic than GR nanosheets towards *Artemia* nauplii and adult of *Artemia.* Hence, both experimental setup proved that the performed nanomaterials have more toxic to *Artemia* culture even at very lowest concentration.

4. Conclusion

Graphene (GR) and graphene/chitosan nanoparticles (GR/CS NCs) were prepared by a simple and cost efficient method. The study demonstrated that GR/CS NCs inhibited successfully biofilm-forming strains of *P. aeruginosa* and K. pneumoniae, more efficiently than GR alone. The CLSM results proved that GR/CS NCs disturbed biofilm aggregation via membrane damage. SEM images by contrast, revealed that the inhibition of biofilm aggregation in both tested strains was due to the disruption of cellular morphology. Additionally, GR/CS NCs showed highly lethal effects towards *A. nauplii* at low concentrations of 70 and 50 µg/mL. Given the biological properties as well as low costs of the starting materials, the prepared GR/CS NCs offer potential for the use as implantable systems to prevent bacterial biofilm development and to control urinary infections.

5. Ethical consideration

All the samples of this study was approved by the ethics review committee (S. No of IEC Management office: DM/2016/101/55) from the Department of Microbiology, Bharathidasan University, Tiruchirappalli, Tamil Nadu, India. The permission was sought from the hospital and laboratory authorities. The ethical principles of scientific research as well as related national laws and regulations were adhered to.

Authors Contribution

Dr. Muthuchamy Maruthupandy and Dr. Govindan Rajivgandhi were designed, worked and drafted the manuscript-especially for the synthesis, structural characterization of graphene-chitosan nanoparticles. All the biological activity parts of the manuscript were done by Dr. Shine Kadaikunnan, Dr. Naiyf S. Alharbi, Dr. Jamal M. Khaled, Prof. Wen Jun-Li, Dr. Khalid F. Alanzi. Dr.Thangasamy Veeramani and Dr. Thillaichidambaram Muneeswaran were detected the invivo toxicity effect of graphene-chitosan nanoparticles against *Artemia.* Professor. Wen-Jun-Li was helped to take the SEM analysis of graphene-chitosan nanoparticles treated bacteria and also corrected the

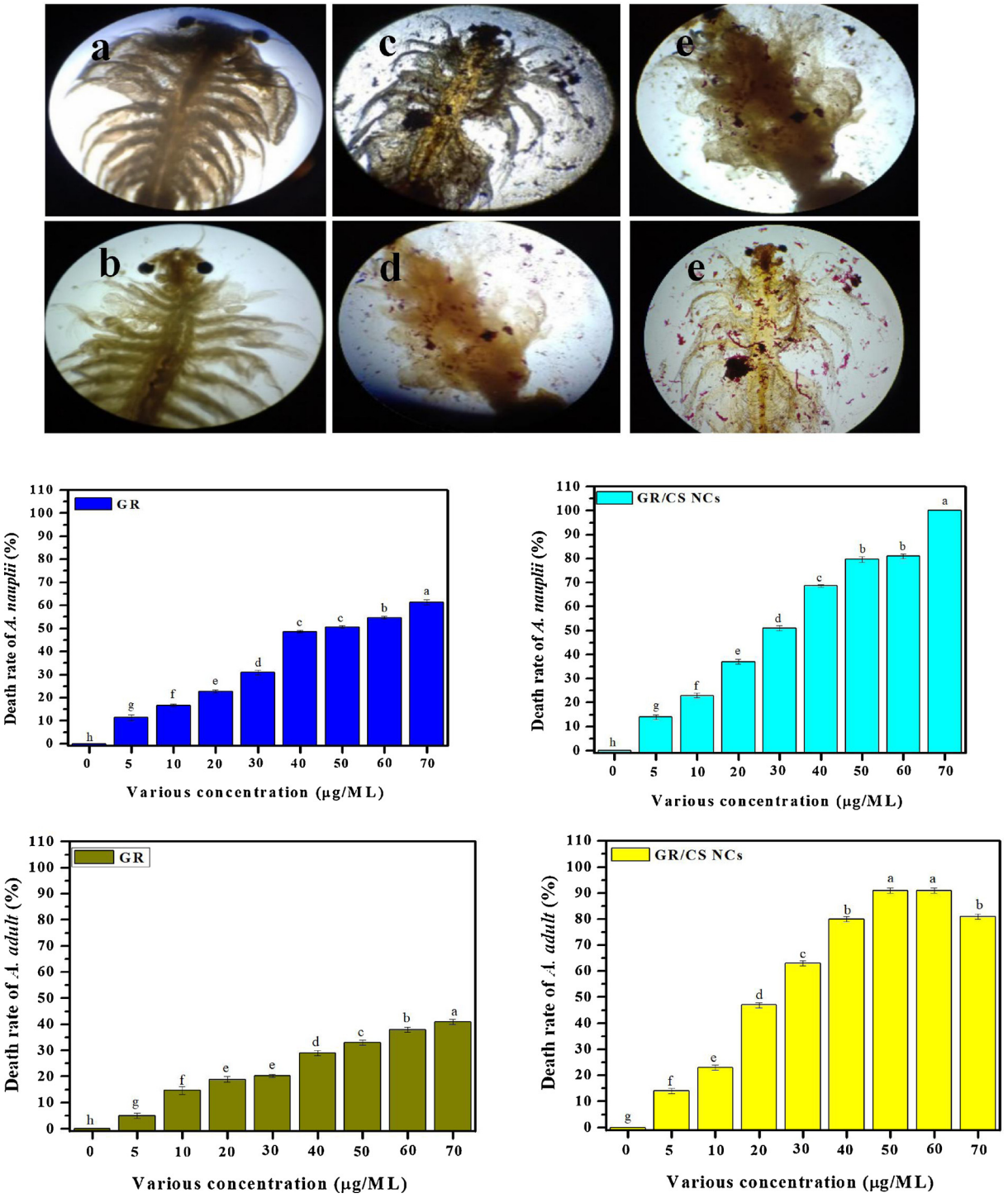

Fig. 9. Evaluation of toxicity effect of GR and GR/CS NCs against *Artemia nauplii* (a,c,e) and effect of GR and GR/CS NCs against *Artemia* adult (b, d, f) based on the mortality. Differentiation of mortality rate due to the increasing concentration at various time interval. 12 h incubation of GR (g), GR-CS NCs (h) and 24 h incubation of GR (i), GR-CS NCs (*j*). All the results were reported as mean ± standard deviation of three independent biological replicates. We employed ANOVA followed by Tukey's HSD test ($P \leq 0.05$) to analysis the data from our antibacterial activity with the help of the SPSS software package 16.0 version.

Grammar, languages in the manuscript.

Declaration of Competing Interest

The authors report no conflicts of interest.

Acknowledgment

All the authors gratefully acknowledge the National Natural Science Foundation of China (Project Approval Number: 41950410573, 91751206) for financial support for this work. The authors would like to acknowledge the financial support from FONDECYT (Chile) under the Postdoctoral Fellowship No. 3180128. The authors also extended their acknowledge to the Deanship of Scientific Research at King Saud

University for funding this work through research group No. RG-1438-074.

References

Abdel Halim, R. M., Kassem, N. N., & Mahmoud, B. S. (2018). Detection of biofilm producing *Staphylococci* among different clinical isolates and its relation to methicillin susceptibility. *Open Access Macedical Journal and Medical Science, 6*, 1335–1341.

Budeli, P., Moropeng, R. C., Mpenyana-Monyatsi, L., & Momba, M. N. B. (2018). Inhibition of biofilm formation on the surface of water storage containers using bios and zeolite silver-impregnated clay granular and silver impregnated porous pot filtration systems. *PloS One, 13*, e0194715.

Cady, N. C., McKean, K. A., Behnke, J., Kubec, R., Mosier, A. P., Kasper, S. H., et al. (2012). Inhibition of biofilm formation, quorum sensing and infection in *Pseudomonas aeruginosa* by natural products-inspired organosulfur compounds. *PloS One, 7*, e38492.

de Moraes, A. C., Lima, B. A., de Faria, A. F., Brocchi, M., & Alves, O. L. (2015). Graphene oxide-silver nanocomposite as a promising biocidal agent against methicillin-resistant *Staphylococcus aureus*. *International Journal of Nanomedicine, 10*, 6847–6861.

Di Giulio, M., Zappacosta, R., Di Lodovico, S., Di Campli, E., Siani, G., Fontana, A., et al. (2018). Antimicrobial and antibiofilm efficacy of graphene oxide against chronic wound microorganisms. *Antimicrobial Agents Chemotheraphy, 62*(7) 547-18.

Divya, M., Vaseeharan, B., Abinaya, M., Vijayakumar, S., Govindarajan, M., Alharbi, N. S., et al. (2018). Biopolymer gelatin-coated zinc oxide nanoparticles showed high antibacterial, antibiofilm and anti-angiogenic activity. *Journal of Photochememistry and Photobiology B, 178*, 211–218.

El-kholany, N. R., Abielhassan, M. H., Elembaby, A. E., & Maria, O. M. (2012). Apoptotic effect of different self-etch dental adhesives on odontoblasts in cell cultures. *Archevies and Oral Biology, 57*(6), 775–783.

Felipe, V., Breser, M. L., Bohl, L. P., Rodrigues da Silva, E., Morgante, C. A., Correa, S. G., et al. (2019). Chitosan disrupts biofilm formation and promotes biofilm eradication in *Staphylococcus* species isolated from bovine mastitis. *International Journal of Biological Macromolecules, 126*, 60–67.

Fernandes, S. C. M., Freire, C. S. R., Silvestre, A. J. D., Pascoal Neto, C., Gandini, A., & Berglund, L. A. (2010). Transparent chitosan films reinforced with a high content of nanofibrillated cellulose. *Carbohydrate Polymers, 81*, 394–401.

Guo, J., Ren, L., Wang, R., Zhang, C., Yang, Y., & Liu, T. (2011). Water-dispersible graphene noncovalently functionalized with tryptophan and its poly (vinyl alcohol) nanocomposite. *Composite Part B: Engineering, 42*, 2130–2135.

Gupta, D., Singh, A., & Khan, A. U. (2017). Nanoparticles as efflux pump and biofilm inhibitor to rejuvenate bactericidal effect of conventional antibiotics. *Nanoscale Research Letters, 12*(454), 1–6.

Gurunathan, S., Han, J. W., Kwon, D. N., & Kim, J. H. (2014). Enhanced antibacterial and anti-biofilm activities of silver nanoparticles against Gram-negative and Gram-positive bacteria. *Nanoscale Research Letters, 9*(373), 1–17.

He, J., Zhu, X., Qi, Z., Wang, C., Mao, X., Zhu, C., et al. (2015). Killing dental pathogens using antibacterial graphene oxide. *ACS Applied Materials & Interfaces, 7*(9), 5605–5611.

Heidari, H., Hadadi, M., Sedigh Ebrahim-Saraie, H., Mirzaei, A., Taji, A., Hosseini, S. R., et al. (2018). Characterization of virulence factors, antimicrobial resistance patterns and biofilm formation of *Pseudomonas aeruginosa* and *Staphylococcus* sp. Strains isolated from corneal infection. *Journal Francais D' Ophtalmology, 18*, 30292–30294.

Hou, H. M., Jiang, F., Zhang, G. L., Wang, J. Y., Zhu, Y. H., & Liu, X. Y. (2017). Inhibition of *Hafnia alvei* H4 biofilm formation by the food additive dihydrocoumarin. *Journal of Food Protection,* 842–847.

Hsu, L. Y., Kwa, A. L., Lye, D. C., Chlebicki, M. P., Tan, T. Y., Ling, M. L., et al. (2008). Reducing antimicrobial resistance through appropriate antibiotic usage in Singapore. *Singapore Medical Journal, 49*, 749–755.

Hu, W., Peng, C., Luo, W., Lv, M., Li, X., Li, D., et al. (2010). Graphene-based antibacterial paper. *ACS Nano, 4*, 4317–4323.

Huang, J., Liu, Y., Yang, L., & Zhou, F. (2019). Synthesis of sulfonated chitosan and its antibiofilm formation activity against *E. Coli* and *S. Aureus*. *International Journal of Biological Macromolecules, 129*, 980–988.

Hummers, W. S., & Offeman, R. E. (1958). Preparation of graphitic oxide. *Journal of the American Chemical Society, 80* 1339-1339.

Ionita, M., & Iovu, H. (2011). Mechanical properties, urea diffusion, and cell cultural response of poly (vinyl alcohol)–chitosan bioartificial membranes via molecular modeling and experimental investigation. *Composite Part B: Engineering, 43*(5), 2464–2470 2011.

Jardón-Valadez, E., Bondar, A. N., & Tobias, D. J. (2014). Electrostatic interactions and hydrogen bond dynamics in chloride pumping by halorhodopsin. *Biochimistry Biophysics Acta, 1837*(12), 1964–1972.

Jeon, G. W., An, J. E., & Jeong, Y. G. (2012). High performance cellulose acetate propionate composites reinforced with exfoliated graphene. *Composite Part B: Engineering, 43*, 3412–3418.

Jia, J., Gai, Y., Wang, W., & Zhao, Y. (2016). Green synthesis of biocompatiable chitosan-graphene oxide hybrid nanosheet by ultrasonication method. *Ultrason Sonochemistry, 32*, 300–306.

Jiang, Y., Gong, J. L., Zeng, G. M., Ou, X. M., Chang, Y. N., Deng, C. H., et al. (2015). Magnetic chitosan-graphene oxide composite for anti-microbial and dye removal applications. *International Journals of Biolological Macromolecules, 82*, 702–710.

Kaiser, T. D., Pereira, E. M., Dos Santo, K. R., Maciel, E. L., Schuenck, R. P., & Nunes, A. P. (2013). Modification of the congo red agar method to detect biofilm production by *Staphylococcus epidermidis*. *Diagnostic Microbiology and Infect Diseases, 75*, 235–239.

Khan, Y. H., Islam, A., Sarwar, A., Gull, N., Khan, S. M., Munawar, M. A., et al. (2016). Novel green nano composites films fabricated by indigenously synthesized graphene oxide and chitosan. *Carbohydrate Polymer, 146*, 131–138.

Konwar, A., Kalita, S., Kotoky, J., & Chowdhury, D. (2016). Chitosan-Iron oxide coated graphene oxide nanocomposite hydrogel: A robust and soft antimicrobial biofilm. *ACS Applied Materials & Interfaces, 8*(32), 20625–20634.

Krajewska, B., Kyzioł, A., & Wydro, P. (2013). Chitosan as a subphase disturbant of membrane lipid monolayers. The effect of temperature at varying pH: II. DPPC and cholesterol. *Colloids and Surfaces A, Physicochemical and Engineering Aspects, 434*, 359–364.

Lau, C., Cooney, M. J., & Atanassov, P. (2008). Conductive macroporous composite chitosancarbon nanotube scaffolds. *Langmuir, 24*, 7004–7010.

Li, L., Wang, Y., Liu, Q., Li, Q., Cheng, Y., Zheng, Y., et al. (2013). In situ synthesis and biocompatibility of nano hydroxyapatite on pristine and chitosan functionalized graphene oxide. *Journal of Materials Chemistry B, 1*, 475–484.

Maruthupandy, M., Rajivgandhi, G., Muneeswaran, T., Song, J.-M., & Manoharan, N. (2018). Biologically synthesized zinc oxide nanoparticles as nanoantibiotics against ESBLs producing gram negative bacteria. *Microbial Pathogenesis, 121*, 224–231.

Nowacka, M., Rygała, A., Kręgiel, D., & Kowalewska, A. (2018). Poly(silsesquioxanes) and poly(siloxanes) grafted with N-acetylcysteine for eradicating mature bacterial biofilms in water environment. *Colloids Surface B Biointerfaces, 172*, 627–634.

Olorunmola, F. O., Kolawole, D. O., & Lamikanra, A. (2013). Antibiotic resistance and virulence properties in *Escherichia coli* strains from cases of urinary tract infections. *African Journal of Infectious Diseases, 7*, 1–7.

Potts, J. R., Dreyer, D. R., Bielawski, C. W., & Ruoff, R. S. (2011). Graphene-based polymer nanocomposites. *Polymer, 52*, 5–25.

Pounraj, S., Prathap, S., & Paul, S. (2018). Chitosan and graphene oxide hybrid nanocomposite film doped with silver nanoparticles efficiently prevents biofouling. *Applied Surface Science, 452*, 487–497.

Prestinaci, F., Pezzotti, P., & Pantosti, A. (2015). Antimicrobial resistance: A global multifaceted phenomenon. *Pathogens and Globel Health, 109*, 309–318.

Raafat, D., & Sahl, H. G. (2009). Chitosan and its antimicrobial potential – A critical literature survey. *Microbial Biotechnology, 2*, 186–201.

Rafiee, M. A., Rafiee, J., Wang, Z., Song, H., Yu, Z. Z., & Koratkar, N. (2009). Enhanced mechanical properties of nanocomposites at low graphene content. *ACS Nano, 3*, 3884–3890.

Rajivgandhi, G., Maruthupandy, M., Muneeswaran, T., Anand, M., & Manoharan, N. (2018). Antibiofilm activity of zinc oxide nanosheets (ZnO NSs) using *Nocardiopsis* sp. GRG1 (KT235640) against MDR strains of gram negative *Proteus mirabilis* and Escherichia coli. *Process Biochemistry, 67*, 8–18.

Rajivgandhi, G., Muneeswaran, T., Maruthupandy, M., Ramakritinan, C. M., Saravanan, K., Ravikumar, V., et al. (2018). Antibacterial and anticancer potential of marine endophytic actinomycetes *Streptomyces coeruleorubidus* GRG 4 (KY457708) compound against colistin resistant uropathogens and A549 lung cancer cells. *Microbial Pathogenesis, 125*, 325–335.

Rajivgandhi, G., Ramachandran, G., Maruthupandy, M., Senthil, R., Vaseeharan, B., & Manoharan, N. (2019). Molecular characterization and antibacterial investigation of marine endophytic actinomycetes *Nocardiopsis* sp. GRG 2 (KT 235641) compound against isolated ESBL producing bacteria. *Microbial Pathogenesis, 126*, 138–148.

Rajivgandhi, G., Vijayarani, J., Kannan, M., Murugan, A., Vijayan, R., & Manoharan, N. (2014). Isolation and identification of biofilm forming uropathogens from urinary tract infection and its antimicrobial susceptibility pattern. *International Journal of Advanced Life Sciences, 7*(2), 352–363.

Rampelotto, R. F., Lorenzoni, V. V., Silva, D. D. C., Coelho, S. S., Wust, V., Garzon, L. R., et al. (2018). Assessment of different methods for the detection of biofilm production in coagulase-negative *staphylococci* isolated from blood cultures of newborns. *Revista da Sociedade Brasilerira de Medicina Tropical, 51*(6), 761–767.

Redgrave, L. S., Sutton, S. B., Webber, M. A., & Piddock, L. J. (2014). Fluoroquinolone resistance: Mechanisms, impact on bacteria, and role in evolutionary success. *Trends in Microbiology, 22*, 438–445.

Santhosh, S. M., & Kandasamy, N. (2015). Antibiofilm Activity of Epoxy/Ag-TiO2 Polymer Nanocomposite Coatings against *Staphylococcus aureus* and Escherichia coli. *Coatings, 5*, 95–114.

Shao, W., Liu, X., Min, H., Dong, G., Feng, Q., & Zuo, S. (2015). Preparation, characterization, and antibacterial activity of silver nanoparticle-decorated graphene oxide nanocomposite. *ACS Applied Materials & Interfaces, 7*, 6966–6973.

Shi, S. F., Jia, J. F., Guo, X. K., Zhao, Y. P., Chen, D. S., Guo, Y. Y., et al. (2016). Reduced *Staphylococcus aureus* biofilm formation in the presence of chitosan-coated iron oxide nanoparticles. *International Journal of Nanomedicine, 11*, 6499–6506.

Sivasubramanian, R., Salini, S., Veera Ravi, A., & Karutha Pandian, S. (2019). Synergistic antibiofilm efficacy of undecanoic acid and auxins against quorum sensing mediated biofilm formation of luminescent *Vibrio harveyi*. *Aquaculture, 498*, 162–170.

Subramaniyan, S. B., Ramani, A., Ganapathy, V., & Anbazhagan, V. (2018). Preparation of self-assembled platinum nanoclusters to combat *Salmonella typhi* infection and inhibit biofilm formation. *Colloids Surface B Biointerfaces, 171*, 75–84.

Syama, S., & Mohanan, P. V. (2016). Safety and biocompatibility of graphene: A new generation nanomaterial for biomedical application. *International Journal of Biological Macromolecules, 86*, 546–555.

Venkatesan, J., & Kim, S. K. (2010). Chitosan composites for bone tissue engineering—An overview. *Marine Drugs, 8*(8), 2252–2266 2010.

Wang, S. F., Shen, L., Zhang, W. D., & Tong, Y. J. (2005). Preparation and mechanical properties of chitosan/carbon nanotubes composites. *Biomacromolecules, 6*, 3067–3072.

Wang, W. X., Wei, Y. W., Li, S. Y., Li, X., Wu, X., Feng, J., et al. (2018). Imaging the dynamics of an individual hydrogen atom intercalated between two graphene sheets. *Physics Revision B, 97*, 085407.

Xu, W., Xie, W., Huang, X., Chen, X., Huang, N., Wang, X., et al. (2017). The graphene oxide and chitosan biopolymer loads TiO_2 for antibacterial and preservative research. *Food Chemistry, 221*, 267–277.

Yadav, N., Dubey, A., Shukla, S., Saini, C. P., Gupta, G., Priyadarshini, R., et al. (2017a). Graphene oxide-coated surface: Inhibition of bacterial biofilm formation due to specific surface-interface interactions. *ACS Omega, 2*, 3070–3082.

Yadav, N., Dubey, A., Shukla, S., Saini, C. P., Gupta, G., Priyadarshini, R., et al. (2017b). Graphene Oxide-Coated Surface: Inhibition of bacterial biofilm formation due to specific surface-interface interactions. *ACS Omega, 2*(7), 3070–3082.

Zavrelova, A., Paterova, P., Gabalec, F., Zak, P., & Radocha, J. (2018). *Ciprofloxacin prophylaxis during autologous stem cell transplantation for multiple myeloma in patients with a high rate of fluoroquinolone-resistant gram-negative bacteria colonization.* Biomedical papers of the Medical Faculty of the University Palacky, Olomouc, Czechoslovakia1–6.

Zhao, S., Zhou, F., Li, L., Cao, M., Zuo, D., & Liu, H. (2012). Removal of anionic dyes from aqueous solutions by adsorption of chitosan-based semi-IPN hydrogel composites. *Composite Part B: Engineering, 43*, 1570–1578.